Transition to Multilayer Kinetic Roughening for Metal (100) Homoepitaxy

M. C. Bartelt[1,3] and J. W. Evans[2,3]
[1]*IPRT, Iowa State University, Ames, Iowa 50011*
[2]*Department of Mathematics, Iowa State University, Ames, Iowa 50011*
[3]*Ames Laboratory, Iowa State University, Ames, Iowa 50011*
(Received 3 January 1995)

A model for metal (100) homoepitaxy is developed which describes irreversible submonolayer nucleation and growth of 2D square islands, and the subsequent transition to multilayer growth. Roughness is sensitive to the additional barrier to descend a step, which is estimated for Fe/Fe(100). We find oscillatory height-height correlations and non-Gaussian height and height-difference distributions, necessitating refinement of existing diffraction theory. We predict the disappearance of a diffraction ring during growth, and a nonmonotonic variation of roughness with temperature.

PACS numbers: 68.55.–a, 68.35.Fx, 82.20.Mj

A central goal of current studies of the structure and kinetic roughening of growing films [1] is to relate the nonequilibrium growth mode to the underlying atomic deposition and diffusion mechanisms, thus allowing control and fabrication of desired nanostructures. Two general paradigms for multilayer film growth and morphology have emerged from continuum Langevin equation theories. The first [1] emphasizes that competition between noise in the deposition flux and surface relaxation processes produces films that have locally both time- and (length) scale-invariant structures, but that roughen globally. Associated critical exponents characterizing local structure and global roughening fall into discrete universality classes. A corresponding diffraction theory has been developed [2] to facilitate interpretation of surface-sensitive diffraction studies. The second paradigm [3,4] is tailored to systems where downward transport (and film roughness) is controlled by a step-edge or Schwoebel barrier E_{Sch}. It predicts "unstable" growth of "mounds," with fixed slope, which coarsen in time according to some universal law.

The validity of these models for describing even "simple" homoepitaxial growth should be scrutinized. For example, despite the above model predictions of universal behavior, roughening of the growing film, and the associated effective exponent, may vary strongly with system parameters and with substrate temperature [5]. Also, existing diffraction theory [2,5,6] incorporates assumptions about the statistics of the film height distribution which we show are often violated. Other basic goals of modeling cannot be met with the Langevin approach, e.g., explaining the observed evolution in the diffraction profile from an initially "split" ring structure, reflecting the characteristic separation of islands nucleated in the submonolayer regime [7], to a nonsplit quasistationary form for rough films [2,5,6,8]. Estimating E_{Sch} is also of prime interest.

In this Letter, we address the above issues via analysis of a model tailored to metal (100) homoepitaxy [5–9]. Our model necessarily incorporates a realistic description of submonolayer nucleation and growth of islands, since this influences subsequent multilayer growth. Film roughness is shown to depend sensitively on E_{Sch}, which is estimated for Fe/Fe(100), and on the downward funneling of depositing atoms to fourfold hollow adsorption sites. Roughness generally increases strongly with decreasing temperature (T), but can diminish again for low T due to downward funneling. We also describe basic features of film morphology displayed by this model, not revealed in previous more idealized studies [1,2]. These include a vertical asymmetry in the film height distribution, oscillations in height correlation functions, and deviations from a Gaussian height-difference distribution (for laterally separated pairs of surface points). Existing diffraction theory [2] fails to incorporate these features. The appropriate refinement is presented, for the first time precisely relating the commonly observed decay of the Bragg intensity oscillations [2] to the height distribution of the roughening film, as well as elucidating the evolution from a split to a nonsplit diffraction profile.

We now describe our simulation model for metal (100) epitaxial growth. Here adatoms reside at fourfold below (4FH) adsorption sites supported by four atoms in the layer beneath. Atoms deposit randomly on the growing surface at a rate $\mathcal{R}$ (measured in ML/s). Those impinging directly at 4FH sites absorb there. Those impinging on top of isolated adatoms, at island edges, or on the sides of microprotrusions, "funnel" or deflect downward until they reach a 4FH site. (See Ref. [10] for details.) Once adsorbed, isolated adatoms undergo intralayer hops between adjacent 4FH sites on the substrate, or on top of islands, at a rate $h = \nu \exp[-E_d/(k_B T)]$. On reaching a descending island edge, an adatom can hop down at a (reduced) rate $h' = \nu \exp[-(E_d + E_{\mathrm{Sch}})/(k_B T)]$. We treat only the regime where adatom bond scission is negligible [7,11]. Thus when diffusing adatoms meet, they irreversibly nucleate islands. When adatoms diffuse across a terrace to an ascending island edge, fall off an island, or are directly deposited adjacent to an island, they are irreversibly

 0031-9007/95/75(23)/4250(4)$06.00

incorporated. Our algorithm then instantaneously restructures the island to maintain a near-square "equilibrium" shape [7]. This mimics rapid transport of edge adatoms to kink sites, a feature specific to metal (100) systems due to a low barrier for edge diffusion. When islands "collide" with other islands as they grow, we preclude restructuring, so they continue to grow as partly overlapping squares [7].

Next we apply our model to analyze STM data for Fe(100) homoepitaxy with $\mathcal{R} = 0.012$ ML/s at 20 °C where island formation is irreversible [8]. We first match the adlayer morphology observed after deposition of $\theta \approx 0.07$ ML of Fe by selecting $E_d \approx 0.45$ eV with $\nu = 10^{12}$/s. STM data [8] for the interface width W (defined below) and layer coverage distributions when $\theta \approx 1$–2 ML are then matched by selecting $E_{\rm Sch} = 45 \pm 5$ meV. (Model behavior is very sensitive to the choice of $E_{\rm Sch}$). With these parameters, we quantitatively reproduce the observed roughening $W \sim \theta^{\beta}$ up to 100 ML, our model prediction of $\beta \approx 0.18$ matching experimental values [6,8]. Similar results are reported in Ref. [12]. Snapshots of the growing film in Fig. 1 reveal the development of disordered "mounds" [3,4] with a vertical asymmetry in the surface morphology: The highest regions are localized tops of mounds, but the lowest are connected channels at their bases, as first observed in Ref. [8]. Figure 2(a) shows the corresponding W versus θ.

We note that significant uncertainty in estimating $E_{\rm Sch}$ is due to the dependence of roughness on model details. Allowing restructuring of islands upon "collision," to form larger squares, enhances next layer nucleation and dramatically lowers the estimate of $E_{\rm Sch}$ (e.g., to $\sim$20 meV if islands of linear dimension $\leq$50 Å can restructure). Also, we estimated $E_{\rm Sch}$ assuming a *uniform* step-edge barrier, but there could be different barriers along straight (110) edges, and at kink sites [13].

Below we analyze real-space and diffraction features of our model. For specificity, we choose the above parameters to match Fe(100) homoepitaxy at 20 °C, but features should be generic to metal (100) homoepitaxy. To simplify the presentation, we suppress some of the complications due to a nonsimple cubic geometry [14,15].

Real-space structure.—We label layers by $j = 0$ (the substrate), $1, 2, \ldots$; θ_j denotes the coverage of layer j, and $P_j = \theta_j - \theta_{j+1}$ the fraction of "exposed" *surface* atoms in layer j. The interface width (in units of the interlayer spacing "b") satisfies $W^2 = \sum_{j\geq 0}(j - j_{\rm av})^2 P_j$, where $j_{\rm av} = \sum_{j\geq 0} jP_j = \theta$. It is convenient to write [10] $P_j \approx W^{-1} f[(j - \theta)/W]$, where f gives the "shape" of the height distribution, and satisfies $\int dx\, f(x) \approx \int dx\, f(x)x^2 \approx 1$ and $\int dx\, f(x)x \approx 0$. While the experimental and simulation P_j data yield roughly Gaussian f, a slight skewness is apparent [cf. Fig. 2(b)]. It corresponds to a *negative* third moment and cumulant $\kappa_3 = \int dx\, f(x)x^3$, which increases in magnitude during growth: $\kappa_3 = -0.15 \pm 0.02$, -0.30 ± 0.04, and -0.45 ± 0.05 for $\theta \approx 5$, 10, and 20 ML in our model. Consequences for Bragg intensity oscillations are discussed below.

The *height-height correlation function* $H(\boldsymbol{\delta\ell})$ gives the mean-square height difference for two surface atoms separated *laterally* [14] by $\boldsymbol{\delta\ell}$ (in units of the separation a

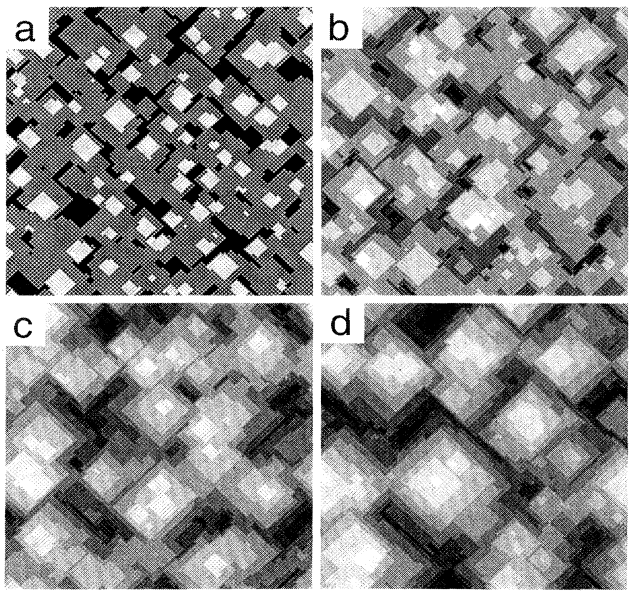

FIG. 1. Simulated film morphology for $E_d \approx 450$ meV, $E_{\rm Sch} \approx 45$ meV, and $\nu \approx 10^{12}$/s at 20 °C, for (a) $\theta = 1$ ML, (b) 5 ML, (c) 25 ML, and (d) 50 ML. Darker regions indicate lower film height.

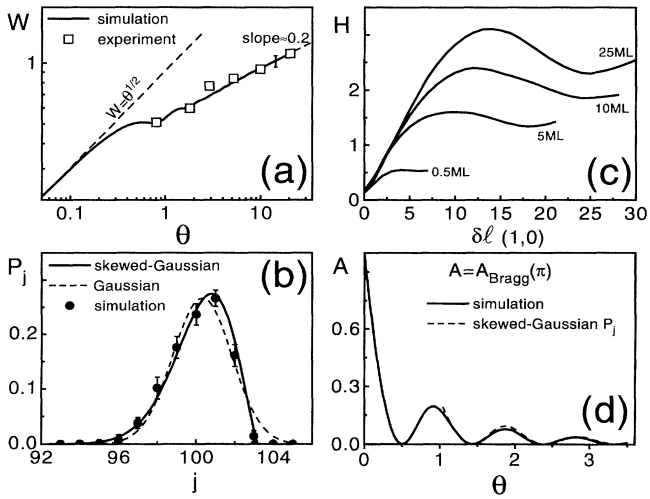

FIG. 2. Simulation results for (a) W vs θ (squares are experimental data [8]); (b) P_j vs j at 100 ML, where $W \approx 1.3$ (circles); Gaussian fit (dashed line) and skewed-Gaussian fit with $\kappa_3 = -2.5$ (solid line); (c) a cross section of $H(\boldsymbol{\delta\ell})$ vs $\boldsymbol{\delta\ell}$ at various θ; (d) $A_{\rm Bragg}(\pi)$ vs θ (solid line); skewed-Gaussian fit [Eq. (3)] with $\kappa_3 = -0.4$ (dashed line).

between 4FH sites), and satisfies [1,2] $H(\boldsymbol{\delta\ell} \to \infty) \to 2W^2$. Simulation data for its evolution are shown in Fig. 2(c). In the submonolayer regime with $\theta_{j\geq 2} \approx 0$, $H(\boldsymbol{\delta\ell})$ first increases linearly, and then slightly overshoots the asymptotic value of $2W^2 \approx 2\theta(1-\theta)$. This overshoot is due to depletion of nearby pairs of islands [7,11]. For $\boldsymbol{\delta\ell}$ slightly larger than the typical island dimension, there is enhanced likelihood of a maximum height difference of unity due to one point coinciding with an island and the other being in the surrounding depletion zone. This overshoot feature is enhanced for multilayer coverages, and decaying oscillations develop, as might be expected for unstable growth producing a disordered array of mounds. The separation at the first maximum measures mound-base size, and increases slowly due to mound coarsening. This $H(\boldsymbol{\delta\ell})$ form differs from the monotonically increasing scaling form [1,2], $H(\boldsymbol{\delta\ell}) \sim 2W^2\{1-\exp[-(\delta\ell/\xi)^{2\alpha}]\}$ for self-affine growth, incorporated into existing diffraction theory.

The diffuse diffraction profiles are determined by the normalized *distribution* $G_n(\boldsymbol{\delta\ell})$ *of height differences* (n), for surface atoms with lateral separation $\boldsymbol{\delta\ell}$. Since $G_n(\boldsymbol{\delta\ell})$ is even in n, with variance $H(\boldsymbol{\delta\ell})$, one can write $G_n(\boldsymbol{\delta\ell}) \approx H(\boldsymbol{\delta\ell})^{-1/2} g[n/H(\boldsymbol{\delta\ell})^{1/2}]$, with *even* g satisfying $\int dy\, g(y) \approx \int dy\, g(y) y^2 \approx 1$. Although G_n (for fixed $\boldsymbol{\delta\ell}$) is typically regarded as Gaussian [2], we find that such a fit is poor for shorter separations, which are most relevant in determining the diffraction profile. A better fit is achieved using a rational form [15], e.g., $g(x) \propto 1/[x^4 + Ax^2 + B]$, even though such distributions do not have all moments finite (contrasting with the exact behavior).

Kinematic diffraction theory.—For lateral momentum transfer $\mathbf{q}$ and vertical momentum transfer $q_\perp$ (with Brillouin zone width 2π), the total kinematic diffracted intensity is given by [2,14]

$$I(\mathbf{q}, q_\perp) = \sum_{\boldsymbol{\delta\ell}} \exp[i\mathbf{q}\cdot\boldsymbol{\delta\ell}] C(q_\perp, \boldsymbol{\delta\ell}) \qquad (1)$$

with

$$C(q_\perp, \boldsymbol{\delta\ell}) = \sum_n \exp[iq_\perp n] G_n(\boldsymbol{\delta\ell}).$$

It is straightforward to show that [15] $C(q_\perp, \infty) = |\sum_{j\geq 0} \exp[iq_\perp j] P_j|^2$, and below we set $\Delta C(q_\perp, \boldsymbol{\delta\ell}) = C(q_\perp, \boldsymbol{\delta\ell}) - C(q_\perp, \infty)$. Near $\mathbf{q} = \mathbf{0}$, the intensity decomposes into *Bragg delta-function* and *diffuse* components, as [2]

$$I(\mathbf{q}, q_\perp) = (2\pi)^2 A_{\mathrm{Bragg}}(q_\perp)\delta(\mathbf{q}) + I_{\mathrm{diff}}(\mathbf{q}, q_\perp), \qquad (2)$$

where $A_{\mathrm{Bragg}}(q_\perp) = C(q_\perp, \infty)$ and $I_{\mathrm{diff}}(\mathbf{q}, q_\perp) = \sum_{\boldsymbol{\delta\ell}} \exp[i\mathbf{q}\cdot\boldsymbol{\delta\ell}] \Delta C(q_\perp, \boldsymbol{\delta\ell})$. We now analyze the behavior of these components separately.

Antiphase Bragg intensity.—For submonolayer θ with $\theta_{j\geq 2} \approx 0$, one has $A_{\mathrm{Bragg}}(\pi) \approx (1-2\theta)^2$. For multilayer growth with "large" W, we evaluate the sum defining $A_{\mathrm{Bragg}}(\pi)$ using the form $P_j \approx W^{-1} f[(j-\theta)/W]$ mentioned above, together with the Poisson summation formula, and a cumulant expansion for f. Here we just report the key result [15,16]

$$A_{\mathrm{Bragg}}(\pi) = 4\cos^2[\pi\theta - \kappa_3\pi^3 W^3/3! + \kappa_5\pi^5 W^5/5! \cdots] \times \exp[-\pi^2 W^2 + 2\kappa_4 \pi^4 W^4/4! \cdots], \qquad (3)$$

where the κ_i are the cumulants of f ($\kappa_1 = 0$ and $\kappa_2 = 1$). Equation (3) provides the first correct description of the characteristic oscillatory decay of $A_{\mathrm{Bragg}}(\pi)$, in contrast to the often quoted formula [2] $A_{\mathrm{Bragg}}(\pi) \approx \exp[-\pi^2 W^2]$. Figure 2(d) shows $A_{\mathrm{Bragg}}(\pi)$ versus θ for our simulation model. The zeros of $A_{\mathrm{Bragg}}(\pi)$ are shifted progressively farther *below* half monolayers, corresponding to the abovementioned skewness $\kappa_3 < 0$ in the height distribution. This feature is reproduced by approximating f as a *skewed* Gaussian.

Diffuse intensity.—In the submonolayer regime where $\theta_{j\geq 2} \approx 0$, all nonzero $G_{n=0,\pm 1}(\boldsymbol{\delta\ell})$ are determined *exactly* by $H(\boldsymbol{\delta\ell})$, as is $\Delta C(q_\perp, \boldsymbol{\delta\ell})$ via

$$\Delta C(q_\perp, \boldsymbol{\delta\ell}) = [H(\infty) - H(\boldsymbol{\delta\ell})][1 - \cos(q_\perp)]. \qquad (4)$$

For multilayer growth with typically "large" $H(\boldsymbol{\delta\ell})$ (and W), the form $G_n(\boldsymbol{\delta\ell}) \approx H(\boldsymbol{\delta\ell})^{-1/2} g[n/H(\boldsymbol{\delta\ell})^{1/2}]$, together with the Poisson summation formula, yields [15]

$$C(q_\perp, \boldsymbol{\delta\ell}) \approx \Delta C(q_\perp, \boldsymbol{\delta\ell}) \approx \hat{g}[[q_\perp] H(\boldsymbol{\delta\ell})^{1/2}], \qquad (5)$$

where $\hat{g}(k) = \int dx\, g(x) \exp[ikx] \to 0$, as $k \to \pm\infty$. Here $[q_\perp]$ means "$q_\perp$ modulo 2π" with $-\pi \leq [q_\perp] \leq \pi$. An extra factor of 2 is required in (5) at the antiphase condition $[q_\perp] = \pm\pi$. We have noted above that g is reasonably fitted by a rational function, which implies that

$$\Delta C(q_\perp, \boldsymbol{\delta\ell}) \approx \exp[-|\mathrm{Im}\lambda[q_\perp]| H(\boldsymbol{\delta\ell})^{1/2}], \qquad (6)$$

where λ is the pole of g closest to the real axis (λ varies little with $\delta\ell$). This form for $\Delta C(q_\perp, \boldsymbol{\delta\ell})$ fits our model well [see Fig. 3(a)], in contrast to the traditional form [2,5,6] for Gaussian g, $\Delta C(q_\perp, \boldsymbol{\delta\ell}) \approx \exp[-[q_\perp]^2 H(\boldsymbol{\delta\ell})/2]$, currently used for diffraction profile analysis.

In Fig. 3(b), we show the evolution from a split to a nonsplit diffuse profile I_{diff} calculated exactly from (1). We explain this behavior as follows. In the *submonolayer* regime, the overshoot in $H(\boldsymbol{\delta\ell})$ produces a corresponding undershoot or "weak oscillation" in $\Delta C(q_\perp, \boldsymbol{\delta\ell})$, obtained from (4), which in turn produces a ring structure [7] in I_{diff}. For *multilayer* growth with "large" W, $H(\boldsymbol{\delta\ell})$ displays a much stronger overshoot and oscillations. But these occur for "large" values of $H \approx O(W^2)$, in the regime of exponentially small $\Delta C(q_\perp, \boldsymbol{\delta\ell})$, which is now determined by (5) rather than by (4). This implies that I_{diff} is insensitive to these oscillations in $H(\boldsymbol{\delta\ell})$, and is determined only by the monotonically increasing short-separation behavior of $H(\boldsymbol{\delta\ell})$, according to (5) or (6). Thus the loss of splitting is a simple consequence of the increase in W.

Finally, we remark on the *temperature dependence* of growth in our model for Fe/Fe(100) homoepitaxy. In the 20 ML range, we find the observed [8] progressively smoother growth (i.e., smaller W) increasing T above 20 °C. However, we also find *reentrant* smooth growth decreasing T below −10 °C. This behavior can be explained within the standard paradigm for unstable growth [3,4]. Reflection of diffusing adatoms from the Schwoebel barrier at descending steps, and biased incorporation at ascending steps, naturally produces an *uphill* current $J_{\rm Sch}$ and thus growth instability. There is also a *downhill* current $J_{\rm DF}$ due to downward funneling [10] at step edges, etc. During growth, the magnitude of the characteristic local slope and the step density increase until $J_{\rm DF}$ counterbalances $J_{\rm Sch}$. As regards the T dependence, for any fixed slope $J_{\rm Sch}$ is reduced at high T due to enhanced Schwoebel barrier crossing, and also at low T where thermal diffuse switches off. On the other hand, the characteristic magnitude of $J_{\rm DF}$ for the growing film is progressively enhanced for lower T due to increasing step density. This effect produces *reentrant* smooth growth.

Clearly, detailed roughening behavior, e.g., β vs T, depends on the system specific values of E_d, which controls island size, and $E_{\rm Sch}$, which controls $J_{\rm Sch}$. For any T regime where the Schwoebel barrier is unsurmountable, film roughness must *increase* with increasing T, since this increases the island size and reduces the influence of $J_{\rm DF}$. If $J_{\rm DF}$ becomes insignificant before the barrier can be surmounted, then "Poisson growth" with $\beta_{\rm max} \approx \frac{1}{2}$ will be observed (cf. Ref. [5]). However, if $J_{\rm DF}$ is significant at this stage, then $\beta_{\rm max}$ will be smaller, as seen in our modeling of Fe/Fe(100) growth.

Our model produces smooth growth with $\beta \to 0$, as $T \to 0$, due to downward funneling [10]. While smooth low-T growth has been observed in several metal (100) epitaxial systems [9], the submonolayer diffraction profiles appear narrower [9] than predicted by our model. We expect this narrowness is due to "clumping" of atoms deposited near other adatoms, rather than to transient mobility [9] of isolated adatoms between 4FH sites. Consequences for roughening as $T \to 0$ will be discussed elsewhere.

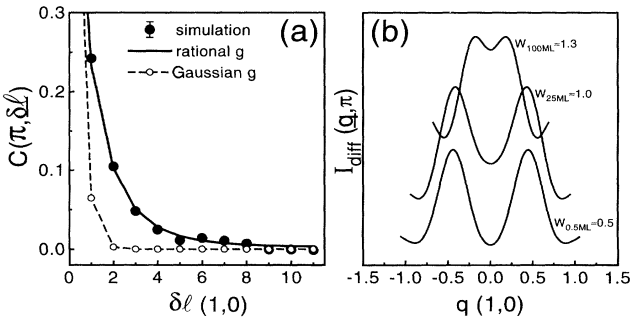

FIG. 3. Simulation results for (a) $C(\pi, \boldsymbol{\delta\ell})$ vs $\boldsymbol{\delta\ell}$ at 100 ML (solid circles); fits shown use Eq. (6) with $|{\rm Im}(\lambda)| \approx 0.8$ (solid line) and the Gaussian approximation (dashed line); (b) evolution of the antiphase diffuse profile.

In conclusion, we have provided a comprehensive description of the transition from submonolayer growth to multilayer kinetic roughening for metal (100) homoepitaxy, allowing estimation of $E_{\rm Sch}$. We have identified deviations from Gaussian height and height-difference distributions, and developed an appropriate theory to describe the key features of diffraction experiments. A nonmonotonic temperature dependence of roughening is also revealed.

This work was supported by NSF Grant No. CHE-9317660. It was performed at Ames Laboratory, which is operated for the USDOE by Iowa State University under contract No. W-7405-Eng-82. We thank J. A. Stroscio for providing unpublished STM data for Fe/Fe(100).

[1] *Dynamics of Fractal Surfaces,* edited by F. Family and T. Vicsek (World Scientific, Singapore, 1991).
[2] H.-N. Yang, G.-C. Wang, and T.-M. Lu, Phys. Rev. Lett. **68**, 2612 (1992); H.-N. Yang, *Diffraction from Rough Surfaces and Dynamic Growth Fronts* (World Scientific, Singapore, 1993).
[3] M. D. Johnson *et al.,* Phys. Rev. Lett. **72**, 116 (1994).
[4] M. Siegert and M. Plischke, Phys. Rev. Lett. **73**, 1517 (1994).
[5] H.-J. Ernst *et al.,* Phys. Rev. Lett. **72**, 112 (1994).
[6] Y.-L. He *et al.,* Phys. Rev. Lett. **69**, 3770 (1992).
[7] M. C. Bartelt and J. W. Evans, Surf. Sci. **298**, 421 (1993); Mater. Res. Soc. Symp. Proc. **312**, 255 (1993).
[8] J. A. Stroscio, D. T. Pierce, and R. A. Dragoset, Phys. Rev. Lett. **70**, 3615 (1993); J. A. Stroscio, D. T. Pierce, M. D. Stiles, A. Zangwill, and L. M. Sander, Phys. Rev. Lett. (to be published).
[9] W. F. Egelhoff and I. Jacob, Phys. Rev. Lett. **62**, 921 (1989); D. K. Flynn-Sanders, J. W. Evans, and P. A. Thiel, J. Vac. Sci. Technol. A **7**, 2162 (1989); Surf. Sci. **289**, 75 (1993).
[10] H. C. Kang and J. W. Evans, Surf. Sci. **271**, 321 (1992); J. W. Evans, Phys. Rev. B **43**, 3897 (1991); J. W. Evans *et al., ibid.* **41**, 5410 (1990). Transient mobility and "knockout" seem inoperative in metal (100) homoepitaxy.
[11] J. A. Venables, Philos. Mag. **27**, 697 (1973).
[12] J. G. Amar and F. Family, Phys. Rev. B **52**, 13 801 (1995).
[13] C. Teichert *et al.,* Phys. Status Solidi A **146**, 223 (1994).
[14] For metal (100) growth, surface atoms are exposed to varying degrees. One takes suitable weighted averages in calculating P_j's, $H(\boldsymbol{\delta\ell})$, etc. We define $\boldsymbol{\delta\ell}$ so that the actual separation between surface atoms with height difference n is $a\boldsymbol{\delta\ell} + nb\hat{\mathbf{z}}$ $(a\boldsymbol{\delta\ell} + nb\hat{\mathbf{z}} + g)$ for n even (odd), with $g = (\frac{1}{2})a(\hat{\mathbf{x}} + \hat{\mathbf{y}})$. Then $\boldsymbol{\delta\ell}$ always has integer components. The expression for $I(\mathbf{q}, q_\perp)$ is also modified [15] from (1).
[15] M. C. Bartelt and J. W. Evans (to be published).
[16] In general, $A_{\rm Bragg}(\pi) \approx 4[{\rm Re}\{e^{-i\pi\theta}\hat{f}(\pi W)\}]^2$, where $\hat{f}(k) = \int dx\, f(x)e^{ikx}$.

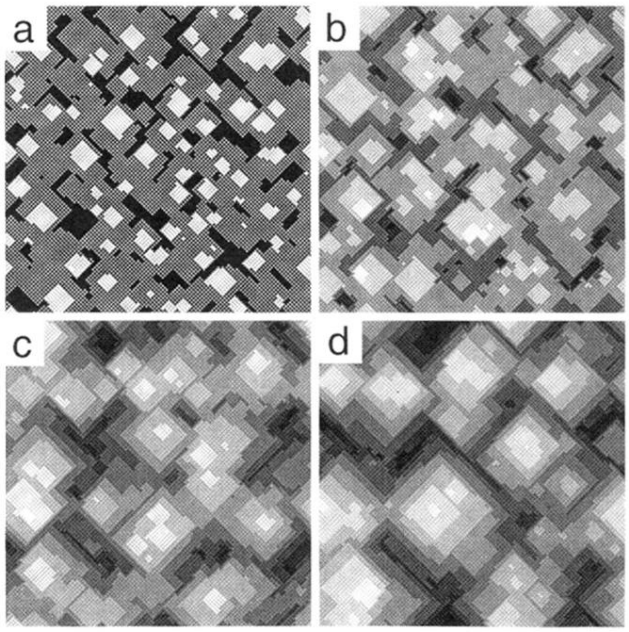

FIG. 1. Simulated film morphology for $E_d \approx 450$ meV, $E_{\mathrm{Sch}} \approx 45$ meV, and $\nu \approx 10^{12}/\mathrm{s}$ at 20 °C, for (a) $\theta = 1$ ML, (b) 5 ML, (c) 25 ML, and (d) 50 ML. Darker regions indicate lower film height.